Nat. Hazards Earth Syst. Sci., 17, 2335–2350, 2017
https://doi.org/10.5194/nhess-17-2335-2017

Natural Hazards and Earth System Sciences
Open Access
EGU

Structural analysis of S-wave seismics around an urban sinkhole: evidence of enhanced dissolution in a strike-slip fault zone

Sonja H. Wadas[1], **David C. Tanner**[1], **Ulrich Polom**[1], **and Charlotte M. Krawczyk**[2,3]

[1]Leibniz Institute for Applied Geophysics, Stilleweg 2, 30655 Hannover, Germany
[2]GFZ German Research Centre for Geosciences, Telegrafenberg, 14473 Potsdam, Germany
[3]Technical University Berlin, Ernst-Reuter-Platz 1, 10587, Germany

Correspondence: Sonja H. Wadas (sonja.wadas@liag-hannover.de)

Received: 31 August 2017 – Discussion started: 4 September 2017
Revised: 9 November 2017 – Accepted: 9 November 2017 – Published: 19 December 2017

Abstract. In November 2010, a large sinkhole opened up in the urban area of Schmalkalden, Germany. To determine the key factors which benefited the development of this collapse structure and therefore the dissolution, we carried out several shear-wave reflection-seismic profiles around the sinkhole. In the seismic sections we see evidence of the Mesozoic tectonic movement in the form of a NW–SE striking, dextral strike-slip fault, known as the Heßleser Fault, which faulted and fractured the subsurface below the town. The strike-slip faulting created a zone of small blocks (<100 m in size), around which steep-dipping normal faults, reverse faults and a dense fracture network serve as fluid pathways for the artesian-confined groundwater. The faults also acted as barriers for horizontal groundwater flow perpendicular to the fault planes. Instead groundwater flows along the faults which serve as conduits and forms cavities in the Permian deposits below ca. 60 m depth. Mass movements and the resulting cavities lead to the formation of sinkholes and dissolution-induced depressions. Since the processes are still ongoing, the occurrence of a new sinkhole cannot be ruled out. This case study demonstrates how S-wave seismics can characterize a sinkhole and, together with geological information, can be used to study the processes that result in sinkhole formation, such as a near-surface fault zone located in soluble rocks. The more complex the fault geometry and interaction between faults, the more prone an area is to sinkhole occurrence.

1 Introduction

Sinkholes are caused by dissolution and subsurface erosion of soluble rocks such as salt, sulfate and carbonate in the presence of water (e.g. groundwater). Fractures and faults can serve as fluid pathways that allow the water to flow through the subsurface and thus generate cavities. A number of authors have pointed out that there is a causal connection between strike-slip faults and sinkholes (Heubeck et al., 2004; Closson and Abou Karaki, 2009; Gabbianelli et al., 2009; Del Prete et al., 2010; Lunina et al., 2016). Strike-slip fault zones with different internal types of fault sense (reverse, normal and strike-slip) are most likely to produce a fine mosaic of small fault blocks that allow groundwater to move freely, thus creating an area of subsidence. Over time, different dissolution structures can occur, e.g. depending on the solubility of the rocks, the hydraulic gradient and the type of the overburden (e.g. soft sediments or solid rock). The two main features that can evolve close to the surface are collapse or depression structures. The former occurs if the overburden is thin enough. The latter is due to slow dissolution (Smyth Jr., 1913; White and White, 1969; Beck, 1988; Martinez et al., 1998; Yechieli et al., 2002; Waltham et al., 2005; Gutiérrez et al., 2008, 2014). Sinkholes can cause damage to buildings and infrastructure and may even lead to life-threatening situations if they occur, for example, in urban areas (Gutiérrez et al., 2014; Parise, 2015).

To determine the causes and the main controlling factors of the sinkhole formation in the urban area of Schmalkalden, a number of investigations were conducted on behalf of the Thuringian State Institute for Environment and Geology (TLUG), including investigation of possible man-

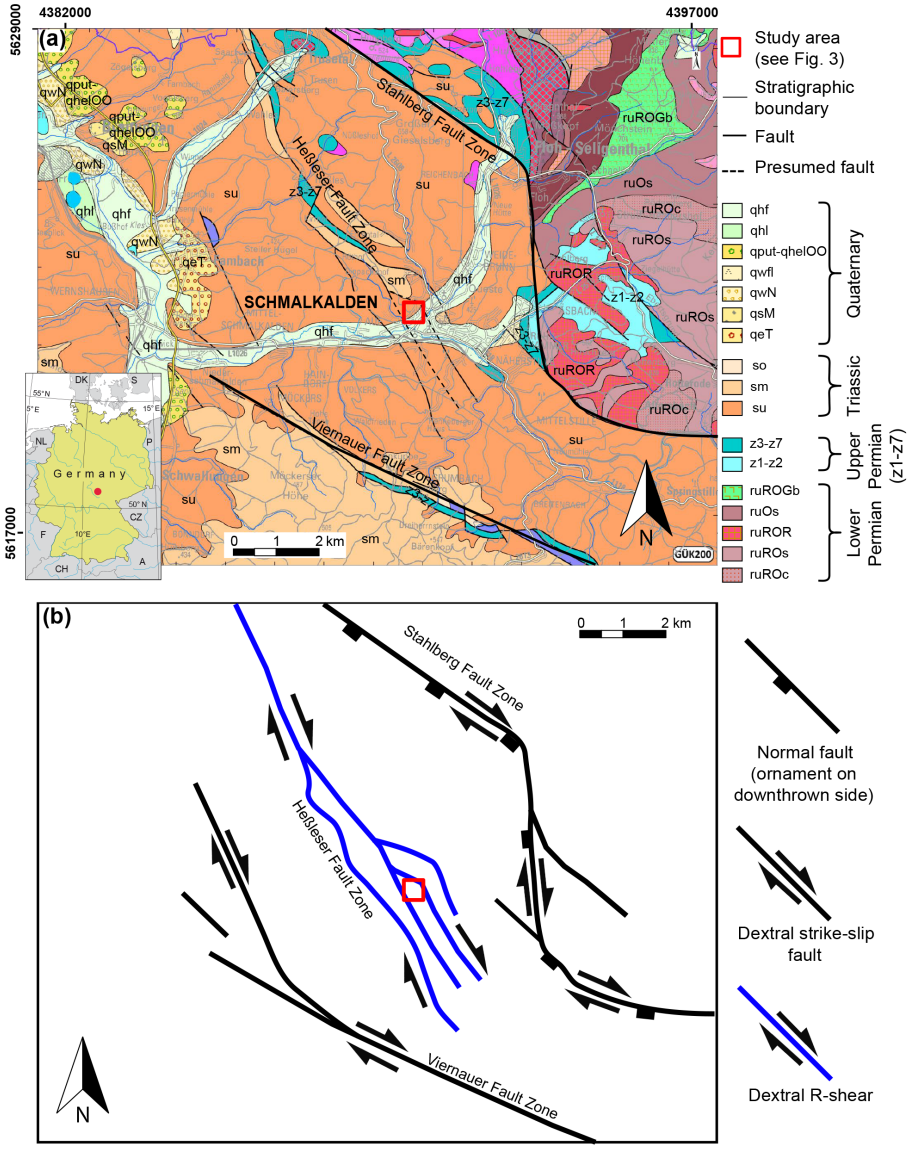

Figure 1. Geological map **(a)** of Schmalkalden and the surrounding areas (after Bücking, 1906), showing the Heßleser Fault zone (HFZ) crossing the position of the sinkhole (red square). In the lower-left corner a map of Germany shows the position of Schmalkalden (red dot). Our interpretation of the fault movement **(b)** is that they were reactivated in the Mesozoic, which led to the formation of a dextral strike-slip fault zone, which includes the Stahlberg Fault zone (SFZ) and the Viernauer Fault zone (VFZ). The HFZ connects the two major faults at an acute angle of 30°. We interpret this as a Riedel R-shear that is also dextral in movement (see text). For an explanation of the stratigraphic abbreviations, see LBEG (2015).

made underground cavities, boreholes, micro-gravimetry, 2-D compression wave (P wave) reflection seismic and hydrological investigations (e.g. chemical composition of the four aquifers) (Schmidt et al., 2013).

The P-wave reflection seismic was unsuccessful at imaging the first ca. 30 m below surface due to a relatively poor resolution, but for instance shear waves (S wave) are able to image the near-surface in high resolution (Dobecki and Upchurch, 2006; Krawczyk et al., 2012; Polom et al., 2016b; Wadas et al., 2016). Interpretation of near-surface faults and structures from the surface down to ca. 100 m depth is important for understanding the local geology and the dissolution-induced structures and processes in general. Therefore, the Leibniz Institute for Applied Geophysics (LIAG) carried out 2-D S_H-wave reflection seismics in this area.

Figure 2. Photographs showing the sinkhole in Schmalkalden that opened up on 1 November 2010. It is 26 to 30 m in diameter and 12 to 17 m in depth (TLUG, 2010).

2 Study area

2.1 Geological evolution

Schmalkalden is located in southern Thuringia, Germany. The deeper bedrock below the research area consists of metamorphic gneiss and micaceous shale, which were deformed during the Variscan orogeny. Later this bedrock was uplifted and formed the Ruhla–Schmalkalden Horst (RSH).

During the upper Permian, the Zechstein Sea transgressed, but due to the horst location, the sediment strata on the RSH are much thinner than elsewhere in the basin. The climatic conditions of the Permian led to a deposition of very thick evaporite. The Zechstein deposits are subdivided into seven sequences, which begin with reef dolomite rocks surrounding the RSH and forming the Werra Formation. The upper part of the Werra Formation is characterized by red claystones which indicate the end of the reef growth (Dittrich, 1966). Sulfate rocks occur above this and form the main horizon prone to dissolution. The following Staßfurt Formation consists of sulfates, claystones and dolomites, whereby over 50 % of the sulfate rocks consist of gypsum, which is why this formation is categorized as part of the dissolution horizon. This formation is followed by the Leine Formation, which contains claystones and carbonates. The upper part of the Zechstein deposits is represented by claystones, sandstones and dolomites of the Leine, Aller, Ohre and Friesland formations, and finishes with sand- and claystones of the Fulda Formation (Schmidt et al., 2012, 2013).

In the study area, the Zechstein Formation is followed by terrestrial sediments of the Triassic, i.e. the Calvörde and Bernburg formations of the Lower Buntsandstein (Fig. 1). Because of intense erosion due to fault movement, mostly since the Upper Cretaceous, which also led to the uplift of the Thuringian Forest, these formations are also the youngest beds to outcrop in the region, except for some Quaternary deposits.

Wunderlich (1997) distinguished six tectonic phases between the Lower Carboniferous and the Tertiary, the last two of which are the most important for this work. From the upper Permian to the Lower Cretaceous the area of Schmalkalden was subject to an extensional stress regime, while from the Upper Cretaceous to the Tertiary it was dominated by a compressional stress regime.

2.2 Faults

Thuringia is crossed by several major NW–SE-striking faults (Wunderlich et al., 1997; Wunderlich, 1997; Andreas and Wunderlich, 1998). Schmalkalden is located to the south of the Stahlberg Fault zone (SFZ). The SFZ is downthrown to the south-west and uplifts basement rocks to the north-east. However, this was accompanied by dextral strike-slip movement, as can be seen from the jogs in the fault trace (Fig. 1). Together with the Viernauer Fault (VFZ) to the south, the SFZ and the VFZ formed a dextral strike-slip fault zone. The Heßleser Fault zone (HFZ) connects the two major faults at an acute angle of 30°. We interpret this as a Riedel R-shear (for definition of a Riedel shear, see Woodcock and Fischer, 1986), also dextral in movement (Fig. 1). Most probably this movement took place during the Upper Cretaceous/early Tertiary inversion phase in Europe (Tanner et al., 1998; Littke et al., 2008; Kley and Voigt, 2008; Tanner and Krawczyk, 2017). The south-eastern part of the HFZ cross-cuts the town of Schmalkalden. The fault zone contains several smaller fault branches that strike NW–SE (Bücking, 1906; Böhne, 1915; Krzywicki, 1937).

2.3 Sinkhole

On 1 November 2010 at 03:00, a large sinkhole opened up in the residential area of Schmalkalden (Fig. 2). The sinkhole was 26 to 30 m in diameter, 12 to 17 m in depth and the crater had a volume of 4000 to 4200 m^3 (Schmidt et al., 2013). Directly after the collapse, groundwater fountains were observed along the sinkhole margins and the sinkhole filled with water, which subsequently slowly seeped away into the ground. The crater became wider due to instability of the sinkhole margins. The bedrock, which was visible within the crater, was strongly fractured and showed small-scale faults and folding of layers. The damage caused by the collapse, such as cracks in houses and streets, was mainly concentrated on the areas north and north-east of the sinkhole. The houses directly besides the sinkhole were temporarily evacuated for safety reasons. New cracks formed due to slope movements along the south-west dipping layers, caused by

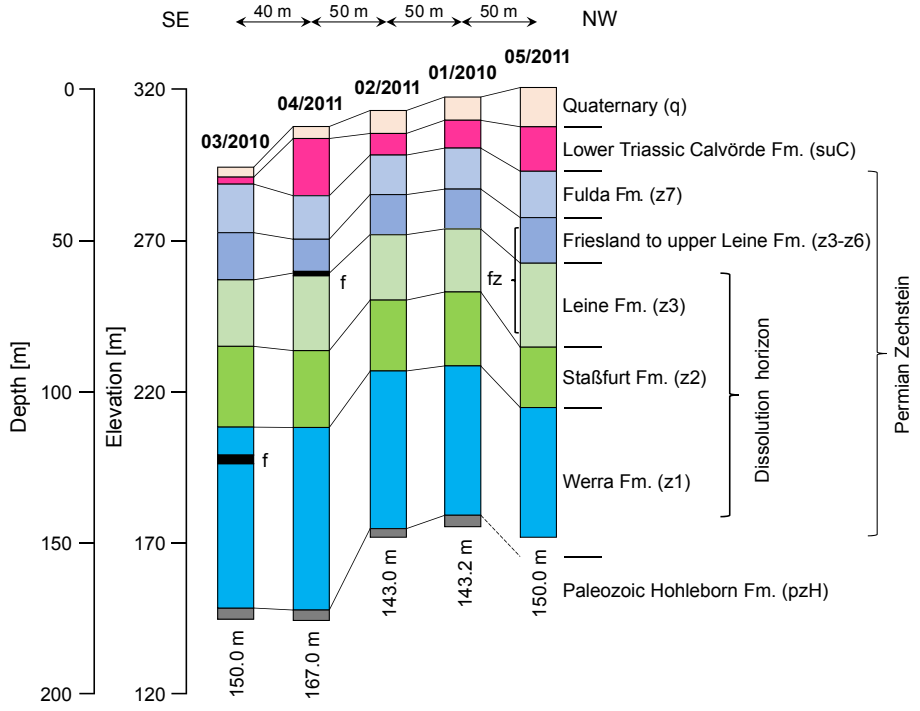

Figure 3. Stratigraphy of the five boreholes (TLUG; personal communication, 2017) near the sinkhole (f is fault, fz is fault zone). The numbers below the profiles show the final depth below surface of each borehole. The stratigraphic units were used for the interpretation of the seismic profiles.

the reduced bedrock stability. To stop slope movement the sinkhole was quickly filled with gravel. On behalf of TLUG, investigations, e.g. archive research, were conducted to determine whether the sinkhole had anthropogenic causes, such as man-made cavities or large underground facilities. However man-made cavities were not found below the sinkhole, and in the vicinity only very small constructions were found, which were not nearly large enough to generate such a large sinkhole (Schmidt et al., 2013). As a result, the sinkhole is probably of natural origin. Although this is the first sinkhole in the urban area of Schmalkalden, several saltwater springs can be found in the surrounding area, which also indicate the long-lasting dissolution processes in this region (Schmidt, 1995; Schmidt et al., 2013).

2.4 Boreholes

To investigate the stratigraphy in the vicinity of the sinkhole in detail, five boreholes with depths of 143 to 167 m were drilled (Fig. 3). In the following, the stratigraphy of the 05/2011 borehole is shown as an example (TLUG, personal communication, 2017). The first 3.55 m consists of anthropogenic deposits, and from 3.55 to 13 m depth, Quaternary terrace gravels and sandy colluvial deposits are found. Between 13 and 28 m depth there are red sandstones of the Triassic Buntsandstein (Calvörde Formation) followed by deposits of the Permian Zechstein. The Zechstein is subdivided into seven formations (see previous section) of which the Fulda Formation (z7) from 28 to 43.45 m depth is the youngest and consists of silty sandstones and claystones (also called "Bröckelschiefer"). Below z7, from 43.45 to 58.60 m, the Aller, Ohre and Friesland formations (z4–z6) and the upper Leine Formation (z3Tb) are found with disturbed clay- and sandstones. Between 58.60 and 86.65 m are disturbed dolomitic lime- and claystones of the lower Leine Formation (z3Ca and z3Ta). The Staßfurt Formation (z2) from 86.65 to 106.85 m depth consists of claystone and gypsum. The oldest Zechstein sequence, the Werra Formation (z1), is found between 106.85 and 150.00 m and consists of a gypsum and anhydrite dissolution breccia, claystone and carbonate. The top of the bedrock, the Paleozoic Hohleborn Formation, was drilled in four other locations (Fig. 3).

Some important results were the discovery of faults and the verification that the dissolution horizon is situated between the base of the Werra Anhydrite (z1) and the base of the Leine Carbonate (z3).

3 Shear wave data

Seven S_H-wave reflection-seismic profiles (total length of ca. 1.3 km) were acquired in the vicinity of the sinkhole in two field campaigns in March 2016 and February 2017 (Fig. 4). To generate horizontally polarized S waves the

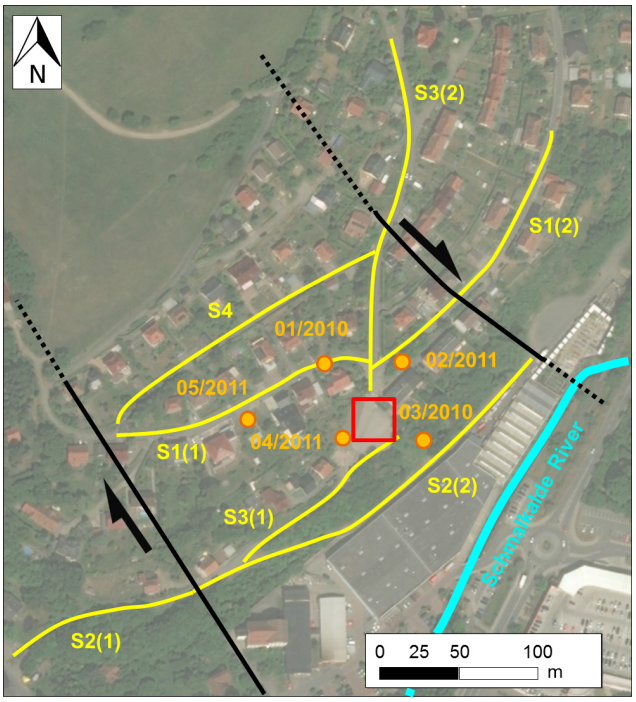

Figure 4. Location map of the S_H-wave reflection-seismic profiles (yellow lines), the boreholes (orange dots), the sinkhole (red square) and the main fault branches of the Heßleser Fault zone (black lines) (ArcGIS, Open Source Map).

Figure 5. Photographs taken during the two field campaigns showing the micro-vibrator, the land streamer and the recording system used for the S_H-wave reflection-seismic surveys.

micro-vibrator ELVIS 7 (Polom, 2003; Druivenga et al., 2011) was used (Fig. 5). The sweep had a duration of 10 s and a frequency range of 20 to 120 Hz. The source spacing was 2 and 4 m, respectively. A receiver array with 112/120 one-component, horizontal geophones at 1 m spacing that was attached to a land streamer was used, and Geometrics Geodes recorded 12 s of raw signal (Fig. 5 and Table A1). A variable split-spread geometry was used with the source and the receivers moving forward. After surveying 60 m, the receivers were moved 60 m forward, while the source moved continuously 2 or 4 m forward. The survey set-up is designed for near-surface reflection-seismic profiling, especially in urban areas, e.g. the suppression of surface Love waves if the first subsurface layer is of higher seismic velocity than the second layer, which is often the case on paved or compacted roads (Polom et al., 2010; Krawczyk et al., 2012). For a successful survey in a karst area the use of a high-frequency signal and a dense receiver and source spacing are important for detecting the strong lateral and vertical, structural variations induced by dissolution and obtaining high-resolution images of the subsurface (Wadas et al., 2016). For more information see Krawczyk et al. (2013) and Polom et al. (2013).

S_H-wave reflection-seismic data processing was carried out using the VISTA software (version 10.028). During preprocessing each record was visually examined for quality assessment, then geometry installation and vibroseis correlation were carried out. This was followed by a 2-fold vertical stack, automatic gain control, normalization and bandpass filter. Afterwards, top mute and spectral balancing were applied, which is important for profiles showing a high frequency attenuation. Surface waves and harmonic distortions covering the desired signal were removed using a frequency wave number (FK) filter. An interactive velocity analysis, normal moveout correction and CMP stack were carried out to generate a seismic section in the time domain. Finally, finite-difference time migration and time-to-depth conversion were applied (Table A2).

4 Results

4.1 Seismic interpretation of S1

S_H-wave reflection-seismic profile S1 of ca. 350 m length, was carried out north of the sinkhole (Fig. 4). At ca. 10 to 25 m depth, a continuous reflector with high amplitude can be traced throughout the entire profile (Fig. 6). The strong impedance contrast represents the boundary between the Triassic sandstones of the Calvörde Formation (suC) and the Permian claystones of the Fulda Formation (z7). This reflector, which can be found in all S_H-wave reflection-seismic profiles, was used as a marker horizon. In contrast, the area beneath shows a mostly discontinuous reflection pattern with no remarkable reflector, although lateral amplitude variations are observed due to strongly fractured strata within the seven Zechstein formations.

In the area north-west of the sinkhole, shallowly dipping reflectors form a bowl-shaped structure of ca. 150 m length and 50 m depth within the Triassic and Permian deposits. In this area the Calvörde Formation shows local thickening. Nu-

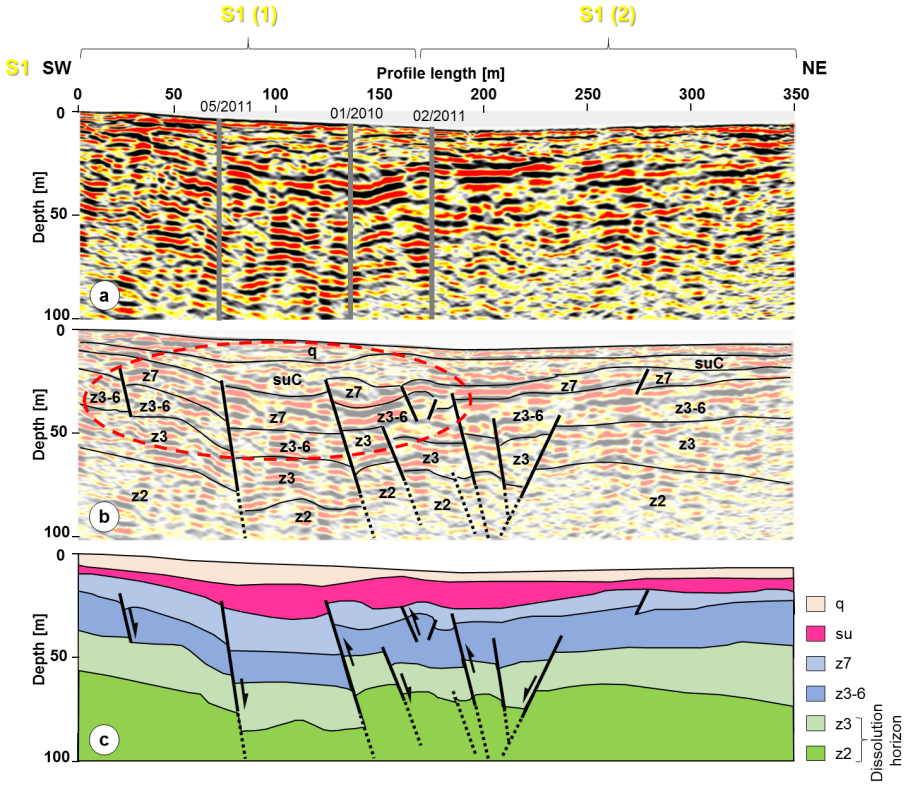

Figure 6. Uninterpreted reflection-seismic profile S1 **(a)** with stratigraphy derived from boreholes 05/2011, 01/2010 and 02/2011 **(b)** and with interpretation **(c)**. The stratigraphic units are explained in Fig. 3. The profile was surveyed north of the sinkhole. Besides local thickening of sediments and thinning of evaporites, several steep-dipping normal and reverse faults within the Permian and Triassic deposits were identified. In the south-west a bowl-shaped structure is visible (red dashed circle), which was interpreted as a dissolution-induced depression.

merous faults in the Zechstein formations with small-scale vertical offsets of ca. 1 to 3 m were identified.

A low-reflectivity zone (LRZ) can be observed at ca. 70 to 100 m depth between 175 and 275 m profile length. This zone shows an almost transparent reflection pattern compared to the neighbouring reflectors at the same depth and is located within the Staßfurt Formation. This correlates with the dissolution horizon within the Zechstein formations of Werra Anhydrite to the Leine Carbonate (z1-z3).

The near-surface in all profiles is represented in detail, with a resolution of less than 1 m at depths down to ca. 15 m and a resolution of ca. 1 to 3 m at 50 m depth.

4.2 Seismic interpretation of S2

S_H-wave reflection-seismic profile S2 of ca. 400 m length was carried out south of the sinkhole (Fig. 4). The marker horizon that represents the base of the Calvörde Formation is clearly visible at ca. 10 to 15 m depth and is traceable throughout the entire profile (Fig. 7). The Permian deposits below show the same discontinuous and disrupted pattern as in profile S1, and numerous fractures were identified.

In the north-eastern area, dipping reflectors form a bowl-shaped structure of ca. 100 m length and 40 m depth within the Triassic and Permian deposits. Below this depression a steep normal fault dipping to the south-west was identified by the reflection-seismic profile and the 03/2011 borehole. South-west of the seismic section other normal and reverse faults with vertical offsets of ca. 5 to 10 m were imaged.

In the Staßfurt Formation, which includes the dissolution horizon, a large LRZ is observed between 175 and 300 m profile length at ca. 70 to 100 m depth below the depression.

4.3 Seismic interpretation of S3

S_H-wave reflection-seismic profile S3 of ca. 370 m length (including a 30 m gap around the sinkhole) was carried out from south to north, passing the sinkhole (Fig. 4). The reflection pattern is similar to S1 and S2.

The flat-lying, mostly continuous reflectors of the Quaternary and the marker horizon of the Triassic Buntsandstein can be precisely identified (Fig. 8). The reflection pattern of the Permian is discontinuous due to vertical displacements of reflectors. Several near-surface normal and reverse faults were identified with fault offsets of ca. 10 to 20 m.

Bowl-shaped structures, as seen in S1 and S2, are not shown, but between ca. 100 and 120 m profile length, an almost transparent area at ca. 40 m depth can be observed. This

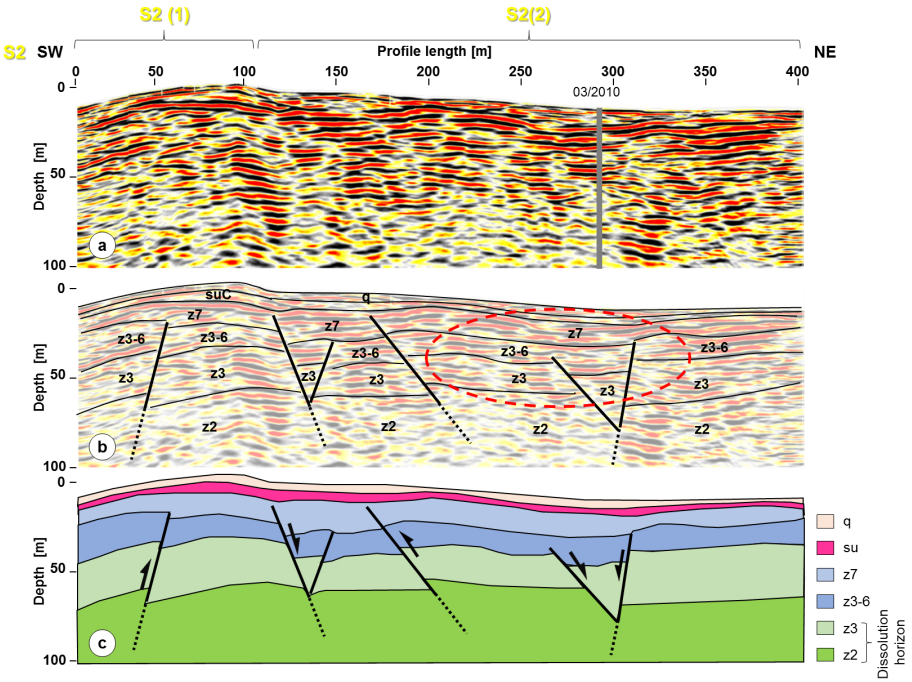

Figure 7. Uninterpreted reflection-seismic profile S2 **(a)**, with stratigraphy derived from the 03/2010 borehole **(b)** and with interpretation **(c)**. The stratigraphic units are explained in Fig. 3. The profile was surveyed south of the sinkhole. Steep-dipping normal and reverse faults within the Permian deposits were identified and in the north-east a bowl-shaped structure (red dashed circle) is visible, which is interpreted as a dissolution-induced depression.

part of S3 was surveyed alongside the filled sinkhole margin. No layers can be identified within the sinkhole zone; the reflectors south of it dip towards the sinkhole. South of this structure, between 80 and 120 m profile length, a northward-dipping steep normal fault was identified in the 04/2011 borehole.

Small LRZs are observed between 240 and 270 m profile length at 70 to 95 m depth.

4.4 Seismic interpretation of S4

S_H-wave reflection-seismic profile S4 of ca. 190 m length, was carried out north-west of the sinkhole (Fig. 4). The Quaternary and the Triassic deposits were identified using the marker horizons and the stratigraphy of the 01/2010 borehole, which was projected onto the seismic line (Fig. 9).

In the north-east and the south-west, within the discontinuous and displaced Zechstein formations, faults with vertical offsets of 5 to 10 m were imaged, which are probably the same as those seen in S1, since S4 runs parallel to the western part of S1. In the same areas, two almost bowl-shaped structures can be identified down to ca. 20 m depth, but they are not as good as visible as the depressions of S1 and S2. In the Zechstein formations z2 to z3 a large LRZ is observed between 60 and 110 m profile length at ca. 60 to 90 m depth.

4.5 Geological interpretation

Combining the information from the geological map, the seismic profiles and the boreholes the following interpretation can be drawn. The subsurface below Schmalkalden has been affected by tectonic movements since at least the Mesozoic, when a NW–SE striking, dextral strike-slip fault zone containing the SFZ and the HFZ formed. The latter crosses the subsurface of the town of Schmalkalden. In the area of the sinkhole, the strike-slip fault created a zone of reverse, normal and strike-slip faults, as shown in the seismic profiles (Fig. 10).

We observe local thickening of the Triassic Calvörde Formation, which can only be accounted for by syntectonic sedimentation during the Triassic. Normal faults generated additional accommodation space for the terrestrial fluvial sediments. This was part of the multiphase tectonic deformation which has been recorded in southern Thuringia (Wunderlich, 1997). The extensional stress regime during the upper Permian to the Lower Cretaceous and the compressional stress regime during the Upper Cretaceous to the Tertiary produced the dextral strike-slip zone and the various strike-slip faults within it. The fine mosaic of fault blocks is mainly attributed to this latter phase.

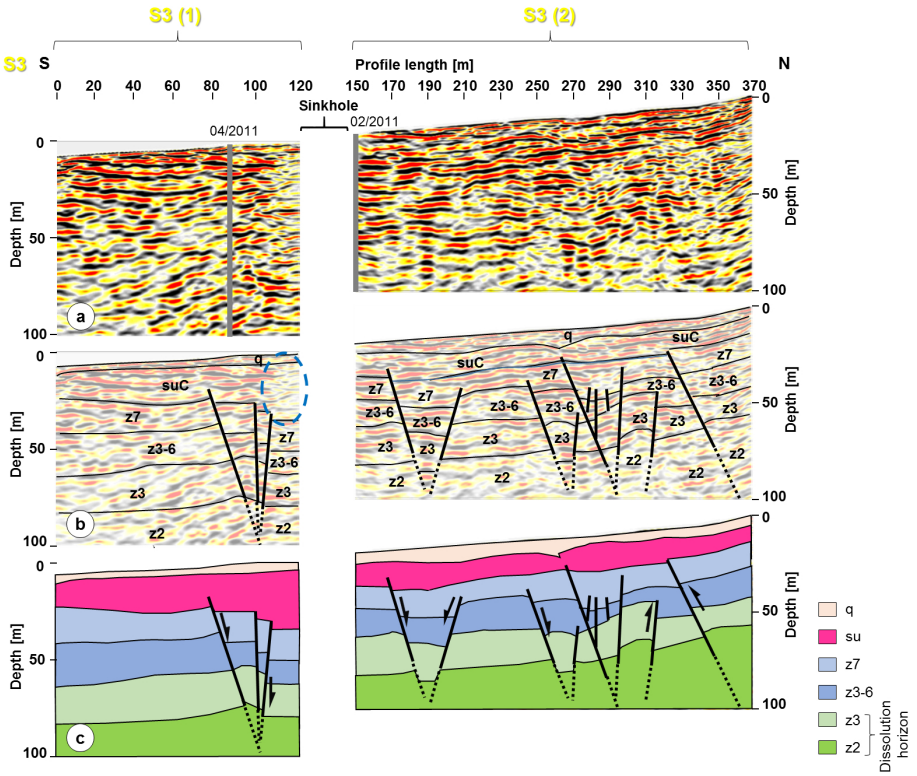

Figure 8. Uninterpreted reflection-seismic profile S3 **(a)** with stratigraphy derived from the 04/2011 and 02/2011 boreholes **(b)** and with interpretation **(c)**. The stratigraphic units are explained in Fig. 3. The profile was surveyed from south to north across the sinkhole area, leaving out the sinkhole itself. Just as in profiles S1 and S2, steep normal and reverse faults can be seen, but no bowl-shaped structure is present. Instead the southern sinkhole margin is visible as a transparent area (blue dashed circle), with near-surface reflectors dipping towards the sinkhole.

4.6 Fault inventory

The complex 3-D structure of the faults is difficult to decipher with 2-D seismic lines, even if they are densely spaced. Nevertheless, large (5 to 10 m) displacements of the reflectors were found at several locations along the profiles, and they are interpreted as near-surface normal and reverse faults; e.g. below the western margin of the depression structure, steep, north-east-dipping reflectors are visible in profile S1 at a depth of 50 to 100 m. The 05/2011 borehole proved the existence of a fault in this zone, which was interpreted as a north-east-dipping normal fault.

Figure 10 shows an overview of all fault positions extrapolated to the surface. The high density of faults means that fault blocks are less than 50 m wide and sometimes less than 10 m, especially directly north of the sinkhole. In general, there is a mixture of apparent normal (25 faults) and reverse (10 faults) faults. All faults have apparent dip angles greater than 70° (apparent angle because they are measured in a 2-D section). This means the seismic profile is close to the true dip direction of the faults, because otherwise the faults would not be so steep. Consequently, the faults strike roughly NW–SE, similar to the strike of the HFZ (Figs. 4 and 10). There is a tendency for normal faults on the south-west end of the profiles to dip north-east and vice versa. Note also that a few faults are outside of the presumed fault zone.

Interestingly, reverse faults cannot be followed from one seismic section to another (e.g. S1 and S4, Fig. 10), meaning that either the strike length of the fault is less than the distance between seismic sections (e.g. less than 50 m), which is most unlikely, or that a reverse fault in one profile correlates with a normal fault in another profile. The significance of this is described in detail in the next section.

5 Discussion

The fact that steep normal and reverse faults occur side by side, as seen in the four seismic sections, could be due to two different mechanisms, both related to strike-slip faults. It is possible that some of the normal faults that were generated under extension during the deformation phase from the upper Permian to the Lower Cretaceous were inverted later by compression during the Upper Cretaceous to the Tertiary (Wunderlich, 1997). For instance, fault bends may switch from transtensional to transpressional systems or vice versa if the original fault bend was at a low angle relative to the

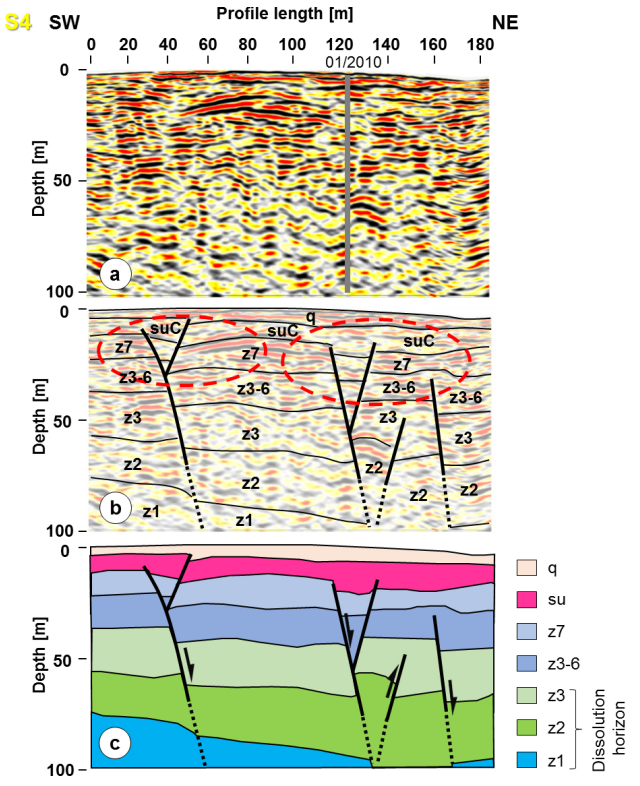

Figure 9. Uninterpreted reflection-seismic profile S4 **(a)** with stratigraphy derived from the 01/2010 borehole **(b)** and with interpretation **(c)**. The stratigraphic units are explained in Fig. 3. The profile was surveyed north of the sinkhole, parallel to S1(1). The normal faults seen in S1 were also identified in S4, while two almost bowl-shaped structures (red dashed circles) are visible in the south-west and the north-east.

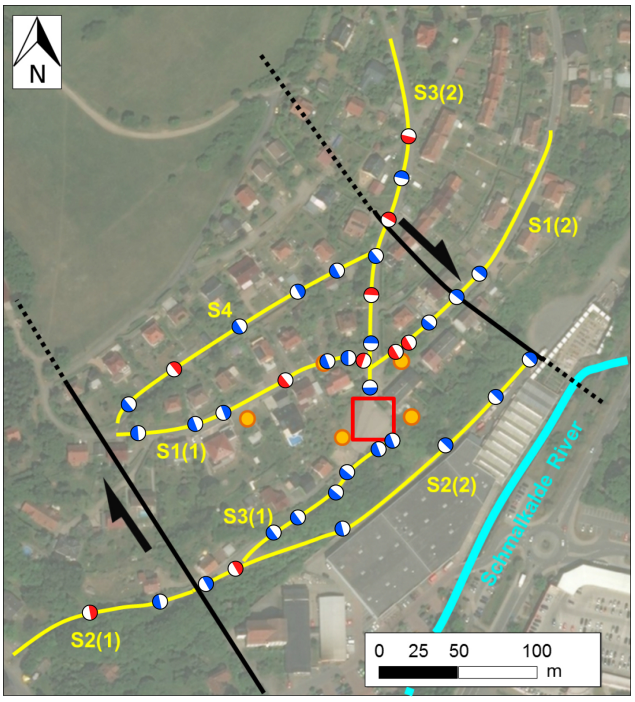

Figure 10. Map showing the complex fault geometry around the sinkhole. The faults identified in the S_H-wave seismic profile were extrapolated to the surface. Blue and red balls represent normal and reverse faults, respectively. The white areas within the balls display the position of the hanging wall. Note the high fault density north of the sinkhole area with fault blocks less than 10 m wide. For borehole information (orange dots), refer to Fig. 3.

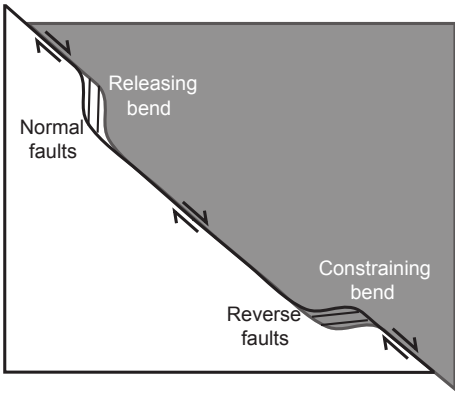

Figure 11. Diagram demonstrating how jogs in a strike-slip fault can cause both constraining and releasing bends. After right-lateral movement, normal and reverse faults are created at the releasing and constraining bends, respectively. The strike of the new faults will be close to that of the strike-slip fault, depending on the original jog angle. Effectively, it creates a system of normal and reverse faults with similar strike, along the strike of the strike-slip fault.

maximum horizontal stress (Tikoff and Teyssier, 1994; Legg et al., 2007). Alternatively, if there are jogs along the strike of a strike-slip fault, this will produce constraining and releasing bends (Cunningham and Mann, 2007), which will cause, after movement, reverse and normal faults, respectively, with strikes similar to the strike-slip fault, along the strike of the strike-slip fault (Crowell, 1974; Christie-Blick and Biddle, 1985; Gamond, 1987, Fig. 11).

The high fault density and the complex fault geometry in the research area (Fig. 10) did not allow a direct spatial correlation of the faults, e.g. connecting the faults that were identified in two 2-D seismic profiles. Only a high-resolution 3-D shear-wave reflection-seismic survey could deliver more or less unquestionable spatial correlations, but such a technique is still in development. Nonetheless, we were able to identify the 2-D fault geometries and displacements from the 2-D reflection-seismic profiles.

The presence of a fault or a fault zone is not the only condition that has to be fulfilled for the occurrence of a sinkhole like that in Schmalkalden. Faults can be classified as open or sealed faults. Fault seal due to clay smear or mineralization could hamper dissolution, because it reduces fluid pathways (Caine et al., 1996; Evans et al., 1997; Ngwenya et al., 2000). On the other hand, an open fault can act as a fluid pathway.

During displacement along a fault, the hanging wall in particular undergoes deformation caused by the fault morphology and the resulting strain variations. The variations in strike of secondary faults are the direct result of these strain variations (Lohr, 2008). These small strike variations can be observed in Schmalkalden, but besides the faults and fractures visible in the seismic sections, subseismic-scale deformation will also have occurred. Displacements along faults can result in a high fracture density around and between faults, creating a damage zone that has the potential to increase the fluid flow due to enhanced permeability. The key factors for the increase in fracture density are the change in mechanical rock properties, interactions between faults and a change in fault geometry (Bolas and Hermanrud, 2003; Gartrell et al., 2004; Leckenby et al., 2005; Eichhubl et al., 2009; Kim and Sanderson, 2010; Ziesch, 2016). The S_H-wave reflection-seismic profiles carried out in this study identified a complex local and regional fault system with a dense fracture network, which enables the groundwater to circulate through the evaporites and therefore it enhances dissolution and subsidence due to an increase in permeability. Different joint sets were observed in outcrops in the vicinity of the sinkhole (Schmidt et al., 2013): (1) steep joints and fracture with a NW–SE strike, (2) flat joints and fractures with a NW–SE strike, (3) NE–SW-striking joints and fractures, (4) young NNE–SSW-striking joints and (5) young NNW–SSE-striking joints.

The sinkhole of Schmalkalden is located at the meeting point of three groundwater catchment areas: the first is to the north and belongs to the Gespringe Spring. The second is ca. 200 m south of the sinkhole and belongs to the confluence of the Schmalkalden River (Fig. 4) with the Stille River. The third is to the west and belongs to the Mittelschmalkalde River. Four groundwater levels are found, in the Quaternary gravel, the Lower Triassic sandstone, the Leine Carbonate (z3) and the Paleozoic bedrock. The latter consists of deep thermal, mineralized water, which is undersaturated with regard to sulfates. This is an indicator of a short residence time and a high hydraulic gradient. The more undersaturated the water, the more sulfates can be dissolved. The main groundwater level situated in the Zechstein formations actively leaches the soluble Permian deposits of the Werra to Leine formations (z1–z3). This Zechstein water ascends along faults and fractures and mixes with water from the upper groundwater levels, since no widespread vertical separation of groundwater levels is available due to tectonics and dissolution (Henke, 1983; Schmidt, 1995). The groundwater movement follows the morphological gradient, and at the steep faults and the intersections of faults the artesian-confined groundwater can migrate upward and leach the soluble Permian deposits. A tracer test revealed a hydraulic gradient of 100 to 150 $m\,h^{-1}$ (Schmidt, 1995), which is a typical value for fractured and karstic aquifer (Ravbar et al., 2012).

Groundwater table contour plans reveal a change in flow direction around the area of the HFZ (Fig. 12). To the north, the groundwater contour lines run from north to south with a flow direction from east to west and from west to east towards the Werra River. In the area of the HFZ, however, the contour lines run approximately east to west with a flow direction from north to south and from south to north towards the Schmalkalde River. This change in groundwater flow direction may be another reason for the occurrence of the sinkhole and can be correlated with the faults discovered in this study, because steep-dipping faults are assumed to be barriers for horizontal groundwater flow perpendicular to the faults but serve as conduits for horizontal flow along the faults (Bredehoeft et al., 1992; Bense et al., 2003). The NW–SE-striking fault branches of the HFZ hamper the groundwater flow coming from the east from the Thuringian Forest towards the Werra River; as a result the water flows from north to south along the faults towards the Schmalkalde River and thereby passes through the sinkhole area.

Several other studies regarding sinkhole distribution have shown the clustering of sinkholes along fault lineaments (Delle Rose and Parise, 2002; Abelson et al., 2003; Doctor et al., 2008; Del Prete et al., 2010) and the decreasing number of sinkhole occurrences with increasing distance from the fault (Hyland et al., 2006; Billi et al., 2007). A lineament of sinkholes can also be used to find hidden faults (Closson and Abou Karaki, 2009). This is the case in Schmalkalden, since the only sinkhole in the urban area formed within the strongly fractured HFZ. A single fault within the soluble rocks might not have influenced the groundwater flow direction and the upward migration of artesian-confined groundwater that much and might not have triggered a collapse due to dissolution and subsurface erosion. Nevertheless, since the soluble rocks are located within a strike-slip fault zone with a typically strongly fractured underground and increased permeability, as described above, the dissolution process is greatly enhanced.

We assume that elongated cavities formed along the fault planes, and at fault intersections these cavities become larger and migrated upward over time. As the sustainability of the overburden is exceeded, the cavity collapses and a sinkhole forms. Additionally, the dissolution-induced depressions within the Quaternary and Triassic deposits and the Zechstein evaporites that are displaced along steep-dipping normal faults and show local thinning, are a result of the leaching processes which occur along the faults. The dissolution rate is most probably very slow. For northern Germany, which is affected by the dissolution of salt, the dissolution rate is mostly less than 1 mm per year (Köthe et al., 2007), and since sulfate rocks have a even lower solubility, the dissolution rate in Schmalkalden is probably much lower than this. Such a determination requires a numerical modelling approach that includes information, e.g. groundwater flow models, mass balance calculations, geomorphological analyses, geochemical investigations of the soluble rocks and the groundwater and fracture evolution (Augarde et al., 2003;

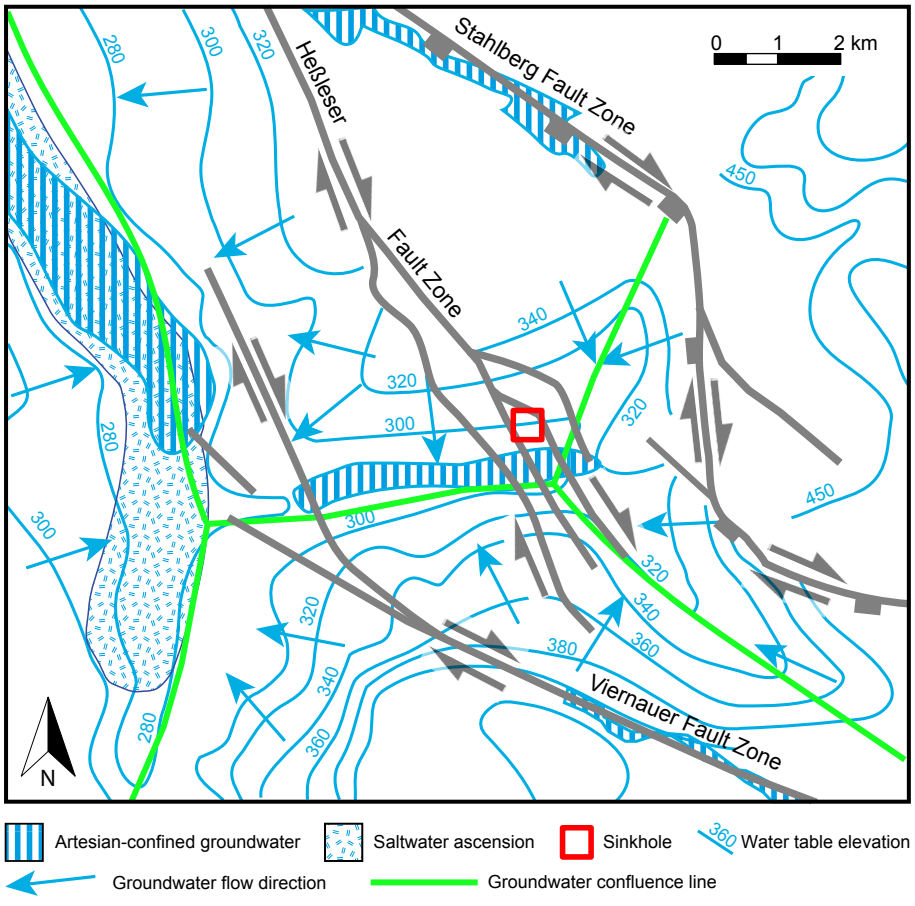

Figure 12. Groundwater table contour map (after TLUG, 2017) reveals a confluence zone of three different groundwater bodies. Three groundwater bodies show different flow routes towards the sinkhole area, and the change in groundwater flow can be seen to correlate with the faults.

Pohl, 2011; Schneider-Löbens et al., 2015). To date, a numerical model does not exist for the sinkhole of Schmalkalden.

Possible indicators of unstable zones and dissolution processes are the LRZs observed in the seismic data. They are visible at the depth of the dissolution horizon and below dissolution-induced features such as depressions. A LRZ can indicate an area in which the evaporites have already been leached or are being leached due to the contact with groundwater. This can also be the reason why the dissolution horizon itself does not generate a strong impedance contrast.

Dissolution creates structures at a subseismic scale which cannot be detected because the resolution limit of the S_H-seismic at such depths is about 3 to 4.5 m. In previous work by Krawczyk et al. (2012) and Wadas et al. (2016), carried out in Hamburg and Bad Frankenhausen in Germany, respectively, similar dissolution-induced features were observed. The seismic sections show a lateral and vertical variable reflection pattern with discontinuous reflectors and small-scale fractures formed by dissolution of soluble rocks near the surface.

Besides reflection-seismic surveys, other geophysical investigations were carried out in Schmalkalden on behalf of TLUG, e.g. gravimetry. Gravimetry is sensitive to density and due to the fault-enhanced dissolution the density varies vertically and laterally. The micro-gravimetric surveys show a negative anomaly with a WNW–ESE extension which crosses the sinkhole and the surrounding area (Schmidt et al., 2013). This anomaly can be linked to the fault system that crosses the sinkhole area. The source of the gravimetric anomaly is located at a depth of 50 to 100 m, which coincides with the dissolution horizon (Seidel and Serfling, 2010).

We assume that the dissolution processes are still ongoing, because the key factors that lead to leaching soluble rocks are still present, e.g. the complex strike-slip fault system and the resulting fractured subsurface with its fluid pathways, the soluble rocks and the confluence zone of three groundwater catchment areas. In the seismic section, several depressions were identified that might develop into sinkholes in the future if the cavities reach the surface, e.g. the large depres-

sion north-west of the sinkhole, which also coincides with the WNW–ESE-trending negative gravimetry anomaly.

In summary, we have discussed the discovery of steep, normal and reverse faults in the seismic sections, which are part of a strike-slip fault zone. The faults are positioned very closely, forming a dense fracture network, not only on the seismic scale but also at the subseismic scale. They act as fluid pathways and lead to fault-enhanced dissolution. We describe a LRZ as a possible indicator of an unstable zone and we show that gravimetry measurements confirm our results.

Altogether, shear-wave reflection seismic measured at Schmalkalden has proven to be a suitable method to image and analyse near-surface dissolution structures at high resolution. This is also the case in Hamburg (Krawczyk et al., 2012), Bad Frankenhausen (Wadas et al., 2016) in Germany and at the Dead Sea in Jordan (Polom et al., 2016a). The method is applicable to other study areas if its limitations are kept in mind, such as the lower penetration depth with respect to P-wave refection seismic, especially in dissolution areas, and the limits of resolution. We suggest it should be used to support P-wave reflection seismics to obtain more structural information in areas where the P wave has insufficient resolution.

6 Conclusions

In this study we used S_H-wave reflection seismic to analyse dissolution features and the link between faults, groundwater flow and soluble rocks.

Areas affected by tectonic deformation phases are prone to enhanced dissolution. The deformation of the fault blocks leads to the generation of a damage zone around and in between the faults with a dense fracture network, which enables the groundwater to flow through the subsurface and to leach soluble rocks. The more complex the fault geometry and the more interaction between faults, the more fractures are generated; e.g. dissolution in a strike slip-fault zone with steep normal and reverse faults will be enhanced more than in an area with just a simple normal or reverse fault.

The faults do not only serve as fluid pathways through which groundwater can migrate upward; they also influence the entire groundwater flow. We have shown that, in a sinkhole area with a broad zone of parallel fault branches, steep-dipping faults can act as barriers for horizontal groundwater flow, but also serve as conduits for water to flow parallel to the fault strike, thus causing dissolution. In Schmalkalden, the dissolution horizon in which the cavities are formed is located between the Permian Leine and Werra formations at ca. 70 to 120 m depth. The long-lasting dissolution processes with rates that are probably slow, causes widespread dissolution. The processes are probably still ongoing.

Structural analysis of S-wave seismics is a valuable tool for detecting near-surface faults in order to characterize the faulting in an area and thus whether it is prone to dissolution or not. The reconstruction of strike and dip directions of even small fault blocks can help to better understand the hydrodynamic groundwater conditions, which is another important factor in understanding the dissolution process in general.

Data availability. The seismic data is the property of LIAG. The data are available from the first author upon request. Please contact Sonja H. Wadas for details.

Appendix A: Shear-wave reflection-seismic data

Table A1 shows detailed information about the equipment, the acquisition parameters and geometry used for the S_H-wave reflection-seismic survey carried out around the sinkhole of Schmalkalden. For detailed explanations regarding the equipment for the high-resolution shear wave reflection seismics, see Polom et al. (2010); Krawczyk et al. (2012, 2013); Polom et al. (2013).

The data processing here was based on general processing procedures, as described by Krawczyk et al. (2012) and Pugin et al. (2013). Table A2 shows the processing steps applied to the S_H-wave reflection-seismic profiles. Most of the processing steps were carried out iteratively and were adjusted for each profile to get the best results. For detailed explanations regarding the processing algorithms see Hatton et al. (1986); Lavergne (1989); Baker (1999); Yilmaz (2001).

Table A1. Acquisition parameters of the S_H-wave reflection-seismic surveys.

Acquisition parameters	S_H-wave reflection seismic
Source type	Electrodynamic vibrator ELVIS 7
Source signal	20–120 Hz (10 s; linear)
Source spacing	2/4 m
Receiver type	1C-geophones (horizontal; 10 Hz)
Number of receivers	112/120
Receiver spacing	1 m
Recording system	Geometrics Geode
Record length	12 s uncorrelated
Sampling interval	1 ms
Record number	1446
Profile length	total ca. 1280 m

Table A2. General processing sequence applied to S_H-wave seismic reflection data. Most of the processing was carried out iteratively and each profile is individualized due to the differing data quality of the profiles.

Processing step	S_H-wave reflection seismic
Correlation	Vibroseis-correlation of sweep/recorded signal to compress the time-stretched signal
Geometry	Geometry assignment
Amplitude balancing and frequency filtering	AGC (220 ms length), bandpass filter (16/18–96/98 Hz) and trace energy normalization
Vertical stack	2-fold
Zeroing of traces	Top mute for individual zeroing of amplitudes at the top of the records
Spectral balancing	Bandwidth range 20 Hz, slope 5 Hz, start 16 Hz, end 95 Hz, not applied to all profiles
2-D filter	Frequency wave number (FK) filter (removal of surface waves, harmonic distortions and coherent noise)
Data sorting	Sort to CMP gathers
Velocity analysis	Interactive velocity picking in using semblance, offset gathers and constant velocity stacks (interval 5 to 20 m)
Normal moveout and stack	NMO correction to shift reflection hyperbolas to zero-offset travel times, followed by CMP trace stack
Filter	Remaining noise is removed using a bandpass or FK filter
Migration	FD time migration using smoothed stacking velocities to move dipping reflectors to their true subsurface position and to collapse diffractions
Depth conversion	Conversion from time section to depth section

Competing interests. The authors declare that they have no conflict of interest.

Acknowledgements. We thank our colleague Saskia Tschache and LIAG's seismic data acquisition and technical development team, Jan Bayerle, Eckhardt Großmann, Sven Wedig and Erwin Wagner, for their excellent work during the field surveys. Furthermore we thank Lutz Katzschmann, Sven Schmidt and Ina Pustal from the Thuringian State Institute for Environment and Geology (TLUG), who provided the borehole information and helped to improve the manuscript. We thank the two anonymous referees and the editor, Mario Parise, for their helpful comments.

Edited by: Mario Parise
Reviewed by: two anonymous referees

References

Abelson, M., Baer, G., Shtivelman, V., Wachs, D., Raz, E., Crouvi, O., Kurzon, I., and Yechieli, Y.: Collapse-sinkholes and radar interferometry reveal neotectonics concealed within the Dead Sea basin, Geophys. Res. Lett., 30, 10, 52.1–52.3, https://doi.org/10.1029/2003GL017103, 2003.

Andreas, D. and Wunderlich, J.: Tektonische Verhältnisse am Westthüringer Quersprung (nordwestlicher Thüringer Wald). II.Spät- und postvariszische Entwicklung an der Reifstieg-Störung un die frühe Entwicklungsphase des Ringgau-Fränkischen Lineaments, Beitr. Geol. Thüringen, 5, 39–72, Weimar, Germany, 1998.

Augarde, C. E., Lyamin, A. V., and Sloan, S. W.: Prediction of Undrained Sinkhole Collapse, J. Geotech. Geoenviron., 129, 3, 197–205, https://doi.org/10.1061/(ASCE)1090-0241(2003)129:3(197), 2003.

Baker, G. S.: Processing Near-Surface Seismic Reflection Data: A primer, Course Note Series-Soc. Expl. Geophys., 9, 1–7, https://doi.org/10.1190/1.9781560802020, 1999.

Beck, B. F.: Environmental and engineering effects of sinkholes – the process behind the problems, Environ. Geol., 12, 2, 71–78, https://doi.org/10.1007/BF02574791, 1988.

Bense, V. F., van Balen, R. T., and de Vries, J. J.: The impact of faults on the hydrogeological coditions in the Roer Valley Rift System: An overview, Netherlands J. Geosci., 82, 1, 41–54, https://doi.org/10.1017/S0016774600022782, 2003.

Billi, A., Valle, A., Brilli, M., Faccenna, C., and Funiciello, R.: Fracture-controlled fluid circulation and dissolutional weathering in sinkhole-prone carbonate rocks from central Italy, J. Struct. Geol., 29, 385–395, https://doi.org/10.1016/j.jsg.2006.09.008, 2007.

Böhne, E.: Das Randgebiet des Thüringer Waldes bei Schmalkalden und Steinbach-Hallenberg, Jahrbuch der Preußische Geologische Landesanstalt, 36, 1, 1–173, Berlin, Germany, 1915.

Bolas, H. M. N. and Hermanrund, C.: Hydrocarbon leakage processes and trap retention capacities offshore Norway, Petrol. Geosci., 9, 4, 321–332, https://doi.org/10.1144/1354-079302-549, 2003.

Bredehoeft, J. D., Belitz, K., and Sharp-Hansen, S.: The hydrodynamics of the Big Horn Basin: A study of the role of faults, AAPG Bulletin, 76, 1, 530–546, 1992.

Bücking, H.: Geologische Karte von Preußen und benachbarten deutschen Ländern. Map Blatt Schmalkalden 5228, Preußische Geologische Landesanstalt, Berlin, Germany, 1906.

Caine, J. S., Evans, J. P., and Forster, C. B.: Fault zone architecture and permeability structure, Geology, 24, 11, 1025–1028, https://doi.org/10.1130/0091-7613(1996)024<1025:FZAAPS>2.3.CO;2, 1996.

Christie-Blick, N. and Biddle, K. T.: Deformation and basin formation along strike-slip faults, in: Strike-Slip Deformation, Basin Formation, and Sedimentation, edited by: Biddle, K. T. and Christie-Blick, N., SEPM Special Publications, 37, 1–34, https://doi.org/10.7916/D8708BJJ, 1985.

Closson, D. and Abou Karaki, N.: Salt karst and tectonics: sinkholes development along tension cracks between parallel strike-slip faults, Dead Sea, Jordan, Earth Surf. Process. Landforms, 34, 1408–1421, https://doi.org/10.1002/esp.1829, 2009.

Crowell, J. C.: Origin of late Cenozoic basins of southern California, in: Tectonics and Sedimentation, edited by: Dickinson, W.R. (ed.) SPEM Special Publications, 22, 190–204, 1974.

Cunningham, W. D. and Mann, P.: Tectonics of strike-slip restraining and releasing bends, Geol. Soc. Lond., Sp. Pub., 290, 1–12, https://doi.org/10.1144/SP290.1, 2007.

Delle Rose, M. and Parise, M.: Karst subsidence in South-Central Apulia, Southern Italy, Int. J. Speleol., 31, 181–199, https://doi.org/10.5038/1827-806X.31.1.11, 2002.

Del Prete, S., Iovine, G., Parise, M., and Santo, A.: Origin and distribution of different types of sinkholes in the plain areas of Southern Italy, Geodinam. Ac., 23, 1–3, 113–127, https://doi.org/10.3166/ga.23.113-127, 2010.

Dittrich, E.: Einige Bemerkungen über Rand- und Schwellenausbildungen im Zechstein Südwest-Thüringens, Bericht der deutsch. Gesellsch. f. geolog. Wiss., 11, 185–198, Berlin, Germany, 1966.

Dobecki, T. L. and Upchurch, S. B.: Geophysical applications to detect sinkholes and ground subsidence, The Leading Edge, 25, 3, 336–341, https://doi.org/10.1190/1.2184102, 2006.

Doctor, D. H., Weary, D. J., Orndorff, R. C., Harlow, G. E., Kozar, M. D., and Nelms, D. L.: Bedrock structural controls on the occurrence of sinkholes and springs in the northern Great Valley karst, Virginia and West Virginia, Proceedings of the 11th Multidisciplinary Conference on Sinkholes and the Engineering and Environmental Impacts of Karst, 12–22, available at: https://va.water.usgs.gov/GLOBAL/Doctor_etal_BedrockStructuralControls_2008.pdf (last access: 13 December 2017), 2008.

Druivenga, G., Grossmann, E., Grüneberg, S., Polom, U., and Rode, W.: Transportabler Scherwellenvibrator, Deutsches Patent-und Markenamt, Offenlegungsschrift DE 103 27 757 B4, 2011.

Eichhubl, P., Davatzes, N. C., and Becker, S. P.: Structural and diagenetic control of fluid migration and cementation along the Moab fault, AAPG Bulletin, 93, 5, 653–681, https://doi.org/10.1306/02180908080, 2009.

Evans, J. P., Forster, C. B., and Goddard, J. V.: Permeability of Fault-Related Rocks, and Implications for Hydraulic Structure of Fault Zones, J. Struct. Geol., 19, 11, 1393–1404, https://doi.org/10.1016/S0191-8141(97)00057-6, 1997.

Gabbianelli, G., Antonellini, M., Mancini, F., Stecchi, F., and Castellarin, A.: Sinkhole geohazard in deformed sulphates at Marina di Lesina (Gargano Promontory, Italy): a combination of anthropogenic, lithologic, and structural

causes, EGU General Assembly, Vienna, Austria, 5934, available at: http://meetingorganizer.copernicus.org/EGU2009/EGU2009-5934.pdf, 2009.

Gamond, J.: Bridge structures as sense of displacement criteria in brittle fault zones, J. Struct. Geol., 9, 609–620, https://doi.org/10.1016/0191-8141(87)90146-5, 1987.

Gartrell, A., Zhang, Y., Lisk, M., and Dewhurst, D.: Fault intersections as critical hydrocarbon leakage zones: Integrated field study and numerical modelling of an example from the Timor Sea, Mar. Petrol. Geol., 21, 9, 1165–1179, https://doi.org/10.1016/j.marpetgeo.2004.08.001, 2004.

Gutiérrez, F., Guerrero, J., and Lucha, P.: A genetic classification of sinkholes illustrated from evaporite paleokarst exposures in Spain, Environ. Geol., 53, 5, 993–1006, https://doi.org/10.1007/s00254-007-0727-5, 2008.

Gutiérrez, F., Parise, M., De Waele, J., and Jourde, H.: A review on natural and human-induced geohazards and impacts in karst, Earth-Sci. Rev., 138, 61–88, https://doi.org/10.1016/j.earscirev.2014.08.002, 2014.

Hatton, L., Worthington, M. H., and Malin, J.: Seismic Data Processing-Theory and Practice, Blackwell Scientific Publications, Oxford, UK, 1986.

Henke, J.: Ergebnisbericht DE Volkers VEB Getränke-Lauraquelle Schmalkalden, unpublished reportGesellsch. f. Ingenieur-, Hydro- und Umweltgeologie Nordhausen, 1–81, 1983. Unpublsihed Report – Hydrogeologie Nordhausen, 1–17, Nordhausen, Germany, 1983.

Heubeck, C., Story, K., Peng, P., Sullivan, C., and Duff, S.: An integrated reservoir study of the Liuhua 11-1 field using a high resolution three-dimensional seismic data set, in: Seismic imaging of carbonate reservoirs and systems, AAPG Memoir, 81, 149–168, 2004.

Hyland, S. E., Kennedy, L. M., Younos, T., and Parson, S.: Analysis of sinkhole susceptibility and karst distribution in the northern Shenandoah valley, Virginia: Implications for low impact development (LID) site suitability models, Virginia Water Resources Research Center Special Report, 31, available at: https://vtechworks.lib.vt.edu/bitstream/handle/10919/49477/VWRRC_sr200631.pdf?sequence=1 (last access: 13 December 2017), 2006.

Kim, Y.-S. and Sanderson, D. J.: Inferred fluid flow through fault damage zones based on the observation of stalactites in carbonate caves, J. Struct. Geol., 32, 9, 1305–1316, https://doi.org/10.1016/j.jsg.2009.04.017, 2010.

Kley, J. and Voigt, T.: Late Cretaceous intraplate thrusting in central Europe: Effect of Africa-Iberia-Europe convergence, not Alpine collision, Geology, 36, 11, 839–842, https://doi.org/10.1130/G24930A.1, 2008.

Köthe, A., Hoffmann, N., Krull, P., Zirngast, M., and Zwirner, R.: Description of the Gorleben site, part 2 – Geology of the overburden and adjoining rock of the Gorleben salt dome, BGR-Bundesanstalt für Geowissenschaften und Rohstoffe, available at: https://www.ptka.kit.edu/downloads/ptka-wte-e/Description_Gorleben_Part2_Geology-overburden-adjoining_rock_en.pdf (last access: 13 December 2017), 2007.

Krawczyk, C. M., Polom, U., Trabs, S., and Dahm, T.: Sinkholes in the city of Hamburg-New urban shear-wave reflection seismic system enables high-resolution imaging of subrosion structures, J. Appl. Geophys., 78, 133–143, https://doi.org/10.1016/j.jappgeo.2011.02.003, 2012.

Krawczyk, C. M., Polom, U., and Beilecke, T.: Shear-wave reflection seismics as a valuable tool for near-surface urban applications, The Leading Edge, 32, 3, 256–263, https://doi.org/10.1190/tle32030256.1, 2013.

Krzywicki, E.: Die saxonische Tektonik im südwestlichen Randgebiet des mittleren Thüringer Waldes, Jahrbuch der Preußische Geologische Landesanstalt, 58, 778–838, Berlin, Germany, 1937.

Lavergne, M.: Seismic methods, Éditions Technip, Paris, 1989.

LBEG – Landesamt für Bergbau, Energie und Geologie: Symbolschlüssel Geologie—Symbole für die Dokumentation geologischer Feld- und Aufschlussdaten, Geozentrum Hannover, Germany, available at: www.lbeg.niedersachsen.de/download/74117/SymbolschluesselGeologie.pdf (last access: 13 December 2017), 2015.

Leckenby, R. J., Sanderson, D. J., and Lonergan, L.: Estimating flow heterogeneity in natural fracture systems, J. Volcanol. Geoth. Res., 148, 1–2, 116–129, https://doi.org/10.1016/j.jvolgeores.2005.03.017, 2005.

Legg, M. R., Goldfinger, C., Kamerling, M. J., Chaytor, J. D., and Einstein, D. E.: Morphology, structure and evolution of California Continental Borderland restraining bends, Geol. Soc. Lond., Sp. Pub., 290, 143–168, https://doi.org/10.1144/SP290.3, 2007.

Littke, R., Bayer, U., Gajewski, D., and Nelskamp S.: Dynamics of Complex Intracontinental Basins: The Central European Basin System, Springer, Berlin Heidelberg, 519 p., https://doi.org/10.1007/978-3-540-85085-4, 2008.

Lohr, T.: PhD Thesis: Seismic and sub-seismic deformation on different scales in the NW German Basin, Free University Berlin, Berlin, Germany, available at: http://www.diss.fu-berlin.de/diss/servlets/MCRFileNodeServlet/FUDISS_derivate_000000003465/00_start.pdf (last access: 13 December 2017), 2008.

Lunina, O. V., Gladkov, A. S., Afonkin, A. M., and Serebryakov, E. V.: Deformation style in the damage zone of the Mondy fault: GPR evidence (Tunka basin, southern East Siberia), Russian Geol. Geophys., 57, 1269–1282, https://doi.org/10.1016/j.rgg.2016.08.012, 2016.

Martinez, J., Johnson, K., and Neal, J.: Sinkholes in Evaporite Rocks, Am. Sci., 86, 1, 38–51, https://doi.org/10.1511/1998.17.909, 1998.

Ngwenya, B. T., Elphick, S. C., Main, I. G., and Shimmield, G. B.: Experimental constraints on the diagenetic self-sealing capacity of faults in high porosity rocks, Earth Planet. Sci. Lett., 183, 187–199, https://doi.org/10.1016/S0012-821X(00)00261-2, 2000.

Parise, M.: A procedure for evaluating the susceptibility to natural and anthropogenic sinkholes, Georisk, 8, 4, 272–285, https://doi.org/10.1080/17499518.2015.1045002, 2015.

Pohl, W. L.: Economic Geology: Principles and Practice, Wiley-Blackwell, Hoboken, USA, 2011.

Polom, U.: Schwingungserzeuger für seismische Anwendungen, Deutsches Patent- und Markenamt, Patentschrift Nr. 102 35 126 C1, 2003.

Polom, U., Hansen, L., Sauvin, G., L'Heureux, J.-S., Lecomte, I., Krawcyzk, C. M., Vanneste, M., and Longva, O.: High-resolution SH-wave Seismic Reflection for Characterization of Onshore Ground Conditions in the Trondheim Harbor, Central Norway,

Geophys. Dev. Ser., Advances in Near-surface Seismology and Ground-penetrating Radar – Geophysical Developments Series, 297–312, https://doi.org/10.1190/1.9781560802259.ch18, 2010.

Polom, U., Bagge, M., Wadas, S., Winsemann, J., Brandes, C., Binot, F., and Krawczyk, C. M.: Surveying near-surface depocentres by means of shear wave seismics, First Break, 31, 8, 67–79, 2013.

Polom, U., Alrshdan, H., Al-Halbouni, D., Sawarieh, A., Dahm, T., and Krawczyk, C. M.: Improved Dead Sea sinkhole site characterization at Ghor Al Haditha, Jordan, based on repeated shear wave reflection seismic profiling, EGU General Assembly, Vienna, Austria, 6440, http://meetingorganizer.copernicus.org/EGU2016/EGU2016-6440.pdf (last access: 13 December 2017), 2016a.

Polom, U., Mueller, C., Nicol, A., Villamor, P., Langridge, R. M., and Begg, J. G.: Finding the concealed section of the Whakatane Fault in the Whakatane Township with a shear wave land streamer system: A seismic surveying report, GNS Science Report, 41, available at: http://www.eqc.govt.nz/sites/public_files/3798-Finding-concealed-section-Whakatane-fault-shear-wave-land-streamer.pdf (last access: 13 December 2017), 2016b.

Pugin, A. J.-M., Brewer, K., Cartwrigth, T., Pullan, S. E., Didier, P., Crow, H., and Hunter, J. A.: Near surface S-wave seismic reflection profiling – new approaches and insights, First Break, 31, 49–60, https://doi.org/10.3997/1365-2397.2013005, 2013.

Ravbar, N., Barberá, J. A., Petric, M., Kogovsek, J., and Andreo, B.: The study of hydrodynamic behaviour of a complex karst system under low-flow conditions using natural and artificial tracers (the catchment of the Unica River, SW Slovenia), Environ. Earth Sci., 65, 8, 2259–2272, https://doi.org/10.1007/s12665-012-1523-4, 2012.

Schmidt, L.: Gutachten zur hydrogeologischen Situation Schmalkalden – unpublished report, Gesellsch. f. Ingenieur-, Hydro- und Umweltgeologie Nordhausen, 1–81, 1995.

Schmidt, S., Wunderlich, J., Geletneky, J., and Steinborn, H.: Ergebnisbericht Untersuchungen und Maßnahmen am Erdfall Tiefenort, Unpublsihed Report – Thuringian State Institute for Environment and Geology, 1–151, Jena, Germany, 2012.

Schmidt, S., Wunderlich, J., Peters, A., and Heinke, O.: Ergebnisbericht Ingenieurgeologische Erkundung des Erdfalls vom 01. November 2010 am Rötbergrain in Schmalkalden und Beschreibung des Erdfall Frühwarnsystems, Unpublished Report – Thuringian State Institute for Environment and Geology, 1–179, Weimar, Germany, 2013.

Schneider-Löbens, C., Wuttke, M. W., Backers, T., and Krawczyk, C. M.: Numerical modeling approach of sinkhole propagation using the eXtended FEM code 'roxol', EGU General Assembly 2015, available at: http://meetingorganizer.copernicus.org/EGU2015/EGU2015-12230-2.pdf (last access: 13 December 2017), 2015.

Seidel, K. and Serfling, U.: Zwischenbericht mikrogravimetrische Messungen im Umfeld des Erdfalls Schmalkalden – unpublished report, GGL Geophysik & Geotechnik Leipzig, 1–15, 2010.

Smyth Jr., C. H.: The Relative Solubilities of the Chemical Constituents of Rocks, J. Geol., 21, 2, 105–120, https://doi.org/10.1086/622044, 1913.

Tanner, D. C. and Krawczyk, C. M.: Restoration of the Cretaceous uplift of the Harz Mountains, North Germany: Evidence for the geometry of a thick-skinned thrust, Int. J. Earth Sci., 106, 2963–2972, https://doi.org/10.1007/s00531-017-1475-8, 2017.

Tanner, D. C., Behrmann, J. H., Oncken, O., and Weber, K.: Three-dimensional retro-modelling of transpression on a linked fault system: the Upper Cretaceous deformation on the western border of the Bohemian Massif, Germany, in: Continental transpressional and transtensional tectonics, edited by: Holdsworth, R. E., Strachan, R. A., and Dewey, J. F., Geol. Soc. Lond., Sp. Pub., 135, 275–287, https://doi.org/10.1144/GSL.SP.1998.135.01.18, 1998.

Tikoff, B. and Teyssier, C.: Strain modelling of displacement-field partitioning in transpressional orogens. J. Struct. Geol., 16, 1575–1588, https://doi.org/10.1144/SP290.1, 1994.

TLUG – Thuringian State Institute for Environment and Geology: Ingenieurgeologie – Baugrund – Georisiken, available at: http://www.thueringen.de/th8/tlug/uw_bericht/2011/geologie/ingenieurgeologie/ (last access: 5 May 2017), 2010.

TLUG – Thuringian State Institute for Environment and Geology: Interactive map, available at: http://antares.thueringen.de/cadenza/pages/map/default/index.xhtml;jsessionid=4778CD657615BEDA90C9B6887BF90FE4, last access: 21 June 2017.

Wadas, S. H., Polom, U., and Krawczyk, C. M.: High-resolution shear-wave seismic reflection as a tool to image near-surface subrosion structures – a case study in Bad Frankenhausen, Germany, Solid Earth, 7, 1491–1508, https://doi.org/10.5194/se-7-1491-2016, 2016.

Waltham, T., Bell, F. G., and Culshaw, M.: Sinkholes and Subsidence-Karst and Cavernous Rocks in Engineering and Construction, Springer-Verlag, Berlin, Germany, 2005.

White, E. L. and White, W. B.: Processes of Cavern Breakdown, Nat. Speleo. Soc., 31, 4, 83–96, 1969.

Woodcock, N. H. and Fischer M.: Strike-slip duplexes, J. Struct. Geol., 8, 7, 725–735, 1986.

Wunderlich, J.: Tektonische Verhältnisse am Westthüringer Quersprung (nordwestlicher Thüringer Wald). III. Permosilesische und saxonische Bruchtektonik an der Gehege-Störung, Freiberger Forschungshefte, C 470, 149–177, Freiberg, Germany, 1997.

Wunderlich, J., Andreas, D., and Hähnel, C.: Tektonische Verhältnisse am Westthüringer Quersprung (nordwestlicher Thüringer Wald). I.Flache Überschiebungstektonik im Zuge Spätsaxonischer Transpression am Nordabschnitt der Floh-Asbach-Störung, Beitr. Geol. Thüringen, 4, 101–131, Weimar, Germany, 1997.

Yechieli, Y., Wachs, D., Shtivelman, V., Abelson, M., Onn, C., Raz, E., and Baer, G.: Formation of sinkholes along the shore of the Dead Sea-summary of the first stage of investigation, GSI Curr. Res., 13, 1–6, available at: http://www.gsi.gov.il/_Uploads/178GSI-Curent-Research-vol13.pdf (last access: 13 December 2017), 2002.

Yilmaz, Ö.: Seismic Data Analysis: Processing, Inversion, and Interpretation of Seismic Data Vol. 1, Soc. Explor. Geophys., Tulsa, USA, 2001.

Ziesch, J.: PhD Thesis: Prediction of seismic and sub-seismic deformation to ensure carbon traps in the Otway Basin, Australia, Technical University Berlin, Berlin, Germany, https://doi.org/10.14279/depositonce-5386, 2016.